Appl. Phys. B 75, 59–62 (2002)
DOI: 10.1007/s00340-002-0953-1

Applied Physics B
Lasers and Optics

D. EHRENTRAUT[1,✉]
M. POLLNAU[1]
S. KÜCK[2]

Epitaxial growth and spectroscopic investigation of $BaSO_4 : Mn^{6+}$ layers

[1] Institute of Applied Optics, School of Engineering, Swiss Federal Institute of Technology, 1015 Lausanne, Switzerland
[2] Institute of Laser-Physics, University of Hamburg, Jungiusstrasse 9a, 20355 Hamburg, Germany

Received: 7 January 2002/Revised version: 30 March 2002
Published online: 8 August 2002 •

ABSTRACT We report on the first layer growth of a Mn^{6+}-doped material. Large-size $BaSO_4$ substrates of $10 \times 6 \times 4\,mm^3$ were grown from a LiCl solvent by the flux method. Flat surfaces of undoped $BaSO_4$ were then achieved by use of liquid-phase epitaxy (LPE) from a CsCl–KCl–NaCl solvent. Finally, $BaSO_4 : Mn^{6+}$ layers were grown by LPE with growth velocities of approximately $3\,\mu m\,h^{-1}$, at temperatures of 550–508 °C. Absorption, luminescence, luminescence-excitation and luminescence-decay measurements confirmed the incorporation of manganese solely in its hexavalent oxidation state. This material possesses potential as a near-infrared tunable laser with a wavelength range larger than Ti:sapphire.

PACS 68.55.-a; 81.05.Je; 81.15.Lm

1 Introduction

Because of the weak shielding of the emitting 3*d* orbitals in transition-metal ions and the corresponding strong electron–phonon coupling of these states, 3*d* systems exhibit luminescence with typically several hundred nanometres of spectral bandwidth. Single-crystalline host materials doped with transition-metal ions are, therefore, of interest for applications as tunable lasers [1], short-pulse lasers [2, 3] and coherent broadband light sources [4]. Whereas many transition-metal-ion-doped systems suffer from excited-state absorption, systems with a d^1 electron configuration such as Ti^{3+}, V^{4+}, Cr^{5+} and Mn^{6+} possess only one excited 3*d* level and excited-state absorption into higher-lying 3*d* levels is, therefore, impossible. Nevertheless, excited-state absorption can occur also in d^1 systems owing to transitions into the conduction band and conduction-band-related energy levels. One of these d^1 systems, $Al_2O_3 : Ti^{3+}$ (Ti:sapphire) has become the most successful tunable [5, 6] and short-pulse [2, 3] laser system to date.

Whereas tetrahedrally coordinated V^{4+} does not show any emission [7] and Cr^{5+}-doped materials exhibit radiative quantum efficiencies smaller than 1% at room temperature [8], the d^1 system Mn^{6+} is a very promising ion for a tunable and short-pulse laser system in the near-infrared spectral region. Recently, the Mn^{6+} ion has been doped into single-crystalline materials by the flux-growth method [9] and near-infrared emission was observed in various host lattices [10]. In the $BaSO_4$ host, stimulated emission has been detected in the spectral range 920–1600 nm at room temperature [11], i.e. as a laser material, $BaSO_4 : Mn^{6+}$ can offer a potentially broader wavelength tuning range than Ti:sapphire. However, the size, crystalline quality and doping level of the crystals have as yet not been sufficient for laser experiments.

In this paper, we report on the first growth of Mn^{6+}-doped layers. Because of the promising spectroscopic properties of Mn^{6+} in $BaSO_4$, this host material was chosen as a substrate for the homoepitaxial growth of Mn^{6+}-doped samples of improved size, quality and doping level. Liquid-phase epitaxy (LPE) is a simple, low-cost and convenient method for the growth of these samples, as it allows for the growth of thin layers of a few microns thickness, to be used as planar waveguides, as well as thick layers, to be used as bulk samples. Both geometries are attractive for laser applications.

2 Crystal growth

In general, the homoepitaxial growth of single-crystalline layers consists of two steps, which both strongly influence the layer quality. The first step is the growth of undoped material of high quality and of sufficient geometrical size to be used as a substrate for homoepitaxy. Ideally, the surface of the substrate to be used as an interface for an optical waveguide structure should be atomically flat and free of any crystal defects, which would be preferred sites for the start of crystallization and the propagation of defect growth into the doped layer. The second step is the growth of layers that contain the optically active ion as a dopant. Low supersaturation and low substrate misorientation are necessary to achieve the Frank-Van-der-Merwe mode (layer-by-layer growth). In this case, a uniform doping distribution and low crystalline defect concentration can be expected. The incorporation of impurities will be diminished and, therefore, have no significant influence on the crystal structure or its optical properties.

2.1 *Flux growth of* $BaSO_4$ *substrates*

The crystal symmetry of the baryte-type $BaSO_4$ is orthorhombic, Pnma, with lattice constants $a_0 = 8.878$ Å, $b_0 = 5.450$ Å and $c_0 = 7.152$ Å [12] at 300 K.

✉ Fax: +41-21/693-3701, E-mail: dirk.ehrentraut@epfl.ch

Growth techniques such as melt growth that typically work at higher growth temperatures fail in the case of $BaSO_4$ owing to two reasons. First, $BaSO_4$ has a phase transition at 1090 °C that starts at 1010 °C [13] and, second, a melting point does not exist due to the thermal decomposition of $BaSO_4$ at 1590 °C. Therefore, a promising growth technique for the fabrication of single-crystalline $BaSO_4$ of sufficient size is the flux-growth method by the use of liquid solutions.

In the first step, we grew $BaSO_4$ bulk crystals by the flux method from a LiCl (99.9% purity) solvent. LiCl was used because of the higher growth rate of $BaSO_4$ with this solvent compared to all other group I and group II chlorides investigated [14] and the possibility of growing large crystals within a shorter time. The maximum crystal size achieved was $10 \times 6 \times 4\ mm^3$ in *a*-, *b*- and *c*-directions, which allowed for the subsequent growth of large-size active layers. The temperature region for the growth was 650–480 °C. Temperatures higher than 650 °C increase the vapor pressure in the solution and material starts to evaporate, thereby changing the concentration of $BaSO_4$ and diminishing the crystal quality. 480 °C is the solidification temperature of the solvent [15]. The cooling rate was $1\ K\,h^{-1}$.

Two processes decreased the crystal quality. Firstly, due to the high supersaturation necessary in the initial part of the flux-growth process for the formation of $BaSO_4$ seed crystals, inclusions typically 1–10 μm in size were incorporated into the crystal volume. Secondly, the surfaces were not sufficiently flat because of the following reason: At the end of the growth process, the temperature approaches the solidification temperature of the solvent and fast one-dimensional growth of $BaSO_4$ occurs, resulting in dendrites with typical dimensions of 10 to 20 μm in width and up to 100 μm in length at the crystal surface. Such kinds of structured surfaces are not suitable as optical interfaces for active waveguides.

2.2 *Liquid-phase epitaxy of undoped* $BaSO_4$ *layers*

Therefore, in an intermediate step, we grew undoped $BaSO_4$ on the flux-grown $BaSO_4$ crystals by use of LPE. Figure 1 schematically shows the LPE set-up for the growth of undoped and doped $BaSO_4$ layers. After heating the solution and equilibrating it for up to 10 h to obtain a homogeneous distribution of solute and dopant in the solution, the growth process was performed under normal pressure and atmosphere. The substrate was dipped into the solution and the growth was started by lowering the solution temperature.

LPE works much closer to the thermodynamic equilibrium than the flux-growth method because of the equilibrium saturation at a desired growth temperature and the constant rotation rate, which diminishes the diffusion-layer thickness between the liquid solution and the solid sample surface. In this way, the large dendrites at the surfaces of the flux-grown substrates are dissolved until equilibrium faces remain. In principle, this process at the beginning of the growth is similar to a partial etching process.

We used the additive ternary solvent CsCl–KCl–NaCl (99.99% purities) in its eutectic composition (45.2 : 24.4 : 30.4 mol % [15]) for the LPE of $BaSO_4$ (99.998% purity on metal basis) as well as for the LPE of the active $BaSO_4$:Mn^{6+} layers, as described later. Both layer types were grown

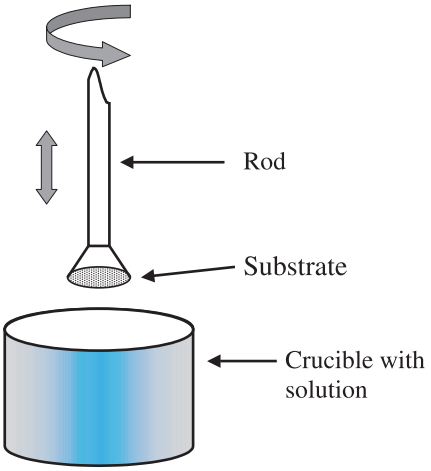

FIGURE 1 Scheme of the LPE set-up that was used when applying rotation during the growth process

under an ambient atmosphere in the temperature region 550–508 °C. The growth process was carried out with a cooling rate of $0.67\ K\,h^{-1}$ and a rotation rate of 10 rpm.

This procedure resulted in *b*- and *c*-oriented undoped $BaSO_4$ layers of approximately 50-μm thickness, with surfaces flat enough for the subsequent growth of high-quality active layers. Figure 2 shows the cross section of a typical $BaSO_4$ layer, homoepitaxially grown on the flux-grown $BaSO_4$ substrate. Large-size inclusions are visible only inside the flux-grown substrate, whereas the LPE-grown layer is free of such inclusions.

2.3 *Liquid-phase epitaxy of* $BaSO_4$**:** Mn^{6+} *layers*

The chemical instability of a desired valence state of the active dopant can pose a major problem for the fabrication of an optically active material. The manganese ion exists in all oxidation states from Mn^{2+} to Mn^{7+}. The divalent state is the most stable oxidation state in neutral solutions [16] such as chloridic salt solvents, however, the stabilities of the different manganese valence states depend strongly

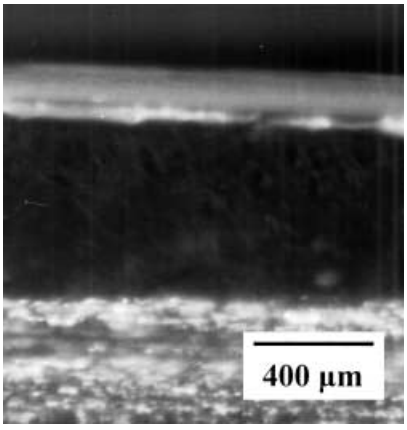

FIGURE 2 Light-microscopic photograph of the cross section of an undoped $BaSO_4$ layer (*upper part*) grown on a $BaSO_4$ substrate (*lower part*), viewed along the *a*-axis. Whereas in the flux-grown substrate inclusions are clearly visible, the layer grown by LPE is free of large-scale scattering centers

on growth temperature and the chemical character of the solution. The choice of an appropriate solvent and control of the growth temperature during the layer-growth process is, therefore, important in order to obtain Mn^{6+}-doped materials. In the baryte-type $BaSO_4$, the Mn^{6+} dopant ion occupies the central S^{6+} site in the SO_4^{2-} tetrahedron. The effective ionic radii of tetrahedrally coordinated S^{6+} and Mn^{6+} in the oxygen coordination are 0.12 and 0.27 Å [17], respectively. The Mn^{6+} ions tend to reduce to Mn^{5+} at temperatures $T \geq 500\,°C$ [18]. At $T \geq 620\,°C$, the Mn^{5+} concentration is high enough to be easily detectable by luminescence spectroscopy [9].

The CsCl–KCl–NaCl solvent used for the LPE of both the undoped and doped $BaSO_4$ layers is completely dissociated in the liquid phase [19]. It has a low solidification temperature of 480 °C under ambient pressure [15] and the growth process could, therefore, be performed at temperatures well below 620 °C. Thus, chemical reduction of the Mn ions was avoided and only Mn^{6+} was incorporated into our layers. K_2MnO_4 (98% purity) was used as the source of the Mn^{6+} dopant ions. Except for providing the Mn^{6+} dopant ions, it does not act as an impurity, because K^+ is also contained in KCl and is, therefore, part of the solvent. Other chloridic alkaline metal and alkaline earth metal solvent systems are less suitable for the growth of $BaSO_4:Mn^{6+}$ owing to higher melting points or chemical reactions with the solute [14].

The nominal Mn^{6+} concentrations were between 0.13 and 0.82 mol % with respect to $BaSO_4$. Although the actual Mn^{6+} concentrations have as yet not been measured in our layers, we expect the distribution coefficient of Mn^{6+} in $BaSO_4$ to be similar to that in $ZnWO_4$, $k = 1.3$ [20]. We grew bulky layers with thickness of up to 580 μm, but a larger thickness can be achieved by repeating the growth process. After cutting and polishing, the thickness of the doped part was measured with a microscope. The growth velocity of each orientation was estimated from the layer thickness and growth duration. The growth velocity varied from 2.8 $\mu m\,h^{-1}$ for *c*-orientation up to 3.7 $\mu m\,h^{-1}$ for *b*-orientation. The layer thickness was controllable with a precision of ±100 nm during the growth process. Besides the possibility of growing bulk samples, these values enable us to fabricate planar sandwich waveguides of a thickness that is precisely controllable by the growth process. This represents an advantage of LPE over many other growth techniques.

Figure 3 shows the result of an atomic-force-microscope (AFM) measurement of the untreated surface of a $BaSO_4:Mn^{6+}$ layer grown on a LPE-grown (001)-$BaSO_4$ substrate. Only flat surface steps are visible. The AFM measurements revealed that these steps are approximately 1.4 nm in height, which corresponds to two unit cells in the *c*-direction, and separated by typically 0.1–0.2 μm. From the AFM measurement we conclude that the growth conditions were not close enough to the thermodynamic equilibrium to demonstrate layer-by-layer growth, but a growth according to the "step-flow" mode was achieved. The particles observed on the layer surface can partly be removed by cleaning. Thus, the optical quality of our samples is expected to be sufficient for use as a laser material. Long-term degradation of the grown surfaces is expected to occur in humid air, because $BaSO_4$ is slightly hygroscopic [21].

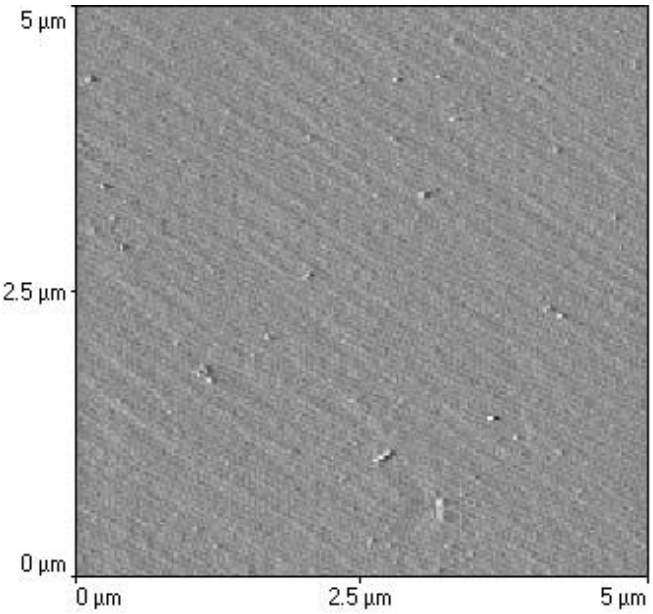

FIGURE 3 As-grown surface of a $BaSO_4:Mn^{6+}$ layer on a (001)-$BaSO_4$ substrate, measured by atomic force microscopy. Step heights of two unit cells and step distances of approximately 100 to 200 unit cells are visible

3 Spectroscopic investigations

In order to confirm the incorporation of the manganese ion in its hexavalent oxidation state, samples of Mn^{6+}-doped $BaSO_4$ layers grown on $BaSO_4$ substrates were investigated spectroscopically by absorption, emission, luminescence-excitation and luminescence-decay measurements at room temperature.

The absorption measurement was carried out with a CARY 2400 spectrophotometer. The spectrum is shown in Fig. 4 (solid line). Its characteristics are similar to the absorption spectrum published earlier by Brunold et al. [11], who identified the optically active center in Mn-doped $BaSO_4$ as the Mn^{6+} ion. The emission (dotted line) and luminescence-excitation (dashed line) spectra of Fig. 4 were measured with a FLUOROG 3 system (Jobin Yvon). The excitation and absorption spectra are similar to each other. The absorption bands are assigned according to Brunold et al. [11] as $^2E \rightarrow {}^2T2$ between 700 and 900 nm and a ligand-to-metal charge-transfer band between 500 and 650 nm. Excitation into these bands leads to the typical Mn^{6+} emission between 850 and 1600 nm [11]. In all three spectra there are no hints of Mn^{5+}. In particular, the sharp features between 8600 and 7200 cm^{-1} that are typical of the emission spectrum of Mn^{5+} [10] do not occur in the emission spectrum of our sample.

The fluorescence decay of $BaSO_4:Mn^{6+}$ at 950 nm was measured after short-pulse excitation at 600 nm by an optical parametric oscillator with 10-ns pulse duration and detected by a S1 photomultiplier. The room-temperature fluorescence lifetime was determined as 0.56 μs. This value is similar to the value of 0.65 μs reported in [9].

In order to estimate the laser potential of $BaSO_4:Mn^{6+}$, we compared the expected pump threshold under continuous-wave excitation with that of Ti:sapphire. The measured peak

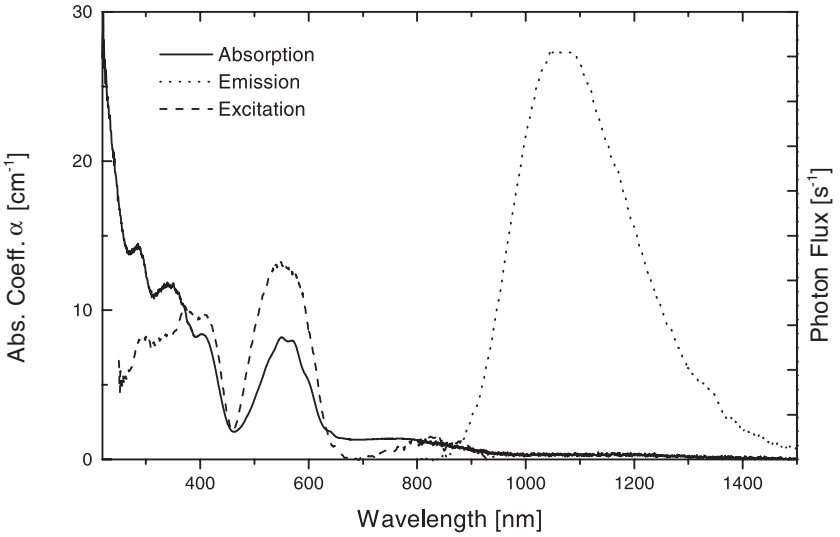

FIGURE 4 Absorption, emission and excitation spectra of a $BaSO_4$:Mn^{6+} layer in the wavelength range 240–1500 nm. The given absorption coefficient is relevant to the whole sample of 2-mm thickness, while the active regions were approximately 175-μm-thick on both surfaces

emission cross section in $BaSO_4$:Mn^{6+} at approximately 1100 nm of $\sigma_{em} = 3 \times 10^{-19}$ cm^2 [11] is slightly smaller than that of Ti:sapphire, 4.5×10^{-19} cm^2 [6]. The fluorescence lifetime of $\tau = 0.6$ μs is a factor of approximately four shorter than in Ti:sapphire, 2.6 μs [22]. The quantum efficiency for lasing at 1100 nm when pumping at 830 nm is $\eta = 75\%$, which is a factor of approximately 1.2 higher than for lasing at 800 nm in Ti:sapphire when pumping at 514 nm. The "figure of merit" for the expected pump threshold under continuous-wave excitation, the product $\sigma_{em}\tau\eta$, is therefore a factor of approximately five smaller than the corresponding value in Ti:sapphire, and the pump threshold will be increased accordingly. In view of this increased threshold, pulsed excitation within a timescale comparable with its fluorescence lifetime could be an interesting alternative to demonstrate laser emission from $BaSO_4$:Mn^{6+}.

4 Conclusions

In this paper, we have demonstrated the first growth of Mn^{6+}-doped $BaSO_4$ layers. Liquid-phase epitaxy close to the thermodynamic equilibrium led to layers of high optical and surface quality, lack of large-size inclusions, low defect concentration and precise control of the layer thickness during the growth process. The low growth temperature led to incorporation of manganese solely in its hexavalent oxidation state, as was confirmed by optical spectroscopy. After further optimization of the growth process and preparation of suitable $BaSO_4$:Mn^{6+} samples, we will investigate the potential of $BaSO_4$:Mn^{6+} for tunable near-infrared laser emission in the wavelength range 920–1600 nm.

ACKNOWLEDGEMENTS The authors thank B. Deveaud-Plédran for his outstanding help with laboratory equipment, R.P. Salathé for his support, G. Jänchen for the AFM measurements, as well as C. Klemenz and T. Brunold for fruitful discussions. This work was partially supported by the Swiss National Science Foundation.

REFERENCES

1 S. Kück: Appl. Phys. B **72**, 515 (2001)
2 I.D. Jung, F.X. Kärtner, N. Matuschek, D.H. Sutter, F. Morier-Genoud, G. Zhang, U. Keller, V. Scheuer, M. Tilsch, T. Tschudi: Opt. Lett. **22**, 1009 (1997)
3 U. Morgner, F.X. Kärtner, S.H. Cho, Y. Chen, H.A. Haus, J.G. Fujimoto, E.P. Ippen, V. Scheuer, G. Angelow, T. Tschudi: Opt. Lett. **24**, 411 (1999)
4 M. Pollnau, R.P. Salathé, T. Bhutta, D.P. Shepherd, R.W. Eason: Opt. Lett. **26**, 283 (2001)
5 P.F. Moulton: J. Opt. Soc. Am. B **3**, 125 (1986)
6 P. Albers, E. Stark, G. Huber: J. Opt. Soc. Am. B **3**, 134 (1986)
7 T.C. Brunold, H.U. Güdel, A.A. Kaminskii: Chem. Phys. Lett. **271**, 327 (1997)
8 M.F. Hazenkamp, H.U. Güdel: J. Lumin. **69**, 235 (1996)
9 T.C. Brunold, H.U. Güdel: Inorg. Chem. **36**, 1946 (1997)
10 T.C. Brunold, H.U. Güdel: Chem. Phys. Lett. **249**, 77 (1996)
11 T.C. Brunold, H.U. Güdel, S. Kück, G. Huber: J. Opt. Soc. Am. B **14**, 2373 (1997)
12 *CRC Handbook of Chemistry and Physics*, 81st edn., ed. by D.R. Lide (CRC Press, Boca Raton 2000)
13 H. Sawada, Y. Takeuchi: Z. Krist. **191**, 161 (1990)
14 D. Ehrentraut, M. Pollnau: J. Cryst. Growth **234**, 533 (2002)
15 The Amer. Ceram. Society Inc.: *Phase Diagrams for Ceramists* (Academic Press, New York 1966)
16 F.A. Cotton, G. Wilkinson: *Advanced Inorganic Chemistry*, 5th edn. (Wiley, New York 1988)
17 A.A. Kaminskii: *Laser Crystals*, *their Physics and Properties*, 2nd edn. (Springer-Verlag, New York, Berlin, Heidelberg 1990)
18 N.V. Sidgwick: *The Chemical Elements and Their Compounds* (University Press, Oxford 1962)
19 Y. Marcus: *Introduction to Liquid State Chemistry* (Wiley, London 1977)
20 A.A. Chernov: *Modern Crystallography III, Crystal Growth* (Springer-Verlag, Berlin, Heidelberg 1984)
21 D. Bosbach, C. Hall, A. Putnis: Chem. Geol. **151**, 143 (1998)
22 S. García-Revilla, F. Rodríguez, R. Valiente, M. Pollnau: J. Phys.: Condens. Matter. **14**, 447 (2002)